Time-domain measurements of surface plasmon polaritons in the terahertz frequency range

J. Saxler, J. Gómez Rivas,* C. Janke, H. P. M. Pellemans, P. Haring Bolívar, and H. Kurz
Institut für Halbleitertechnik, RWTH Aachen, Sommerfeldstrasse 24, D-52056 Aachen, Germany
(Received 29 October 2003; published 28 April 2004)

We present time domain measurements of surface-plasmon polaritons (SPP's) at terahertz (THz) frequencies. SPP's are generated by coupling THz radiation into dielectric films deposited on flat gold surfaces. In this way we are able to perform very sensitive and broadband THz measurements of thin dielectric films, demonstrating the capabilities of SPP's for Thz thin film spectroscopy. By varying the thickness of these films we observe drastic changes in the field distribution of the SPP's.

DOI: 10.1103/PhysRevB.69.155427 PACS number(s): 73.20.Mf, 77.55.+f, 78.20.−e

Surface plasmon polaritons (SPP's) at metal-dielectric interfaces have proven to be a reliable technique for the investigation of thin films, allowing to derive properties such as optical and dielectric constants, film thickness, and inhomogeneities at interfaces with high precision (for an overview see Ref. 1). Additionally, it has been discovered recently that SPP's play a crucial role in the extraordinary high transmission of light through arrays of sub-wavelength holes.[2,3] Thanks to SPP's light can be concentrated and controlled over length scales much smaller than the wavelength. As a result, a new and promising research field known as plasmonics has emerged, one of its primary goals being the fabrication of nanoscale photonic circuits.[4]

With the development of short-pulse lasers terahertz (THz) spectroscopy has opened up an interesting but hardly accessible spectral window where a large variety of gases, liquids, and solids show specific resonances. THz applications range from studies of coherent excitations in semiconductor heterostructures to medical diagnostics and three-dimensional imaging systems for monitoring industrial processes.[5,6] Key biological constituents such as proteins, ribonucleic acids, and deoxyribonucleic acids have resonances at THz frequencies,[7–10] which makes THz radiation of keen interest for direct and simple biosensing. The latter often involves the analysis of typically very thin biomolecular films. Surface plasmon polariton (SPP) spectroscopy at THz frequencies has a large potential for biosensing applications, providing high electromagnetic field strengths in the films together with long interaction lengths.[1] In spite of these important advantages almost no work has been done so far on SPP's in the THz frequency range.[11]

In this paper we present the first time-domain THz study of SPP's on metal surfaces and metals covered with dielectric films. The broadband character of our THz setup allows us to obtain information over a wide range of frequencies between 0.2 and 2 THz in a single measurement. As we will show, small changes on the film thickness relative to the THz wavelength lead to drastic modifications on the SPP's field distribution and spectrum. These modifications demonstrate the capabilities of terahertz SPP's for sensitive spectroscopy of thin films.

Figure 1(a) illustrates the field geometry used for exciting SPP's. A semi-infinite dielectric and a semi-infinite metal define an interface at $z=0$. A p-polarized electromagnetic wave incident from the (y,z) plane is coupled into a surface evanescent wave traveling in the y direction along the interface and decaying exponentially into both media. The magnetic field of the SPP's in the dielectric has the form $\boldsymbol{H}(y,z,t)=\exp(iky-i\omega t)U_e(z)\boldsymbol{e}_x$ with the envelope function[12]

$$U_e(z)=A_1e^{-\beta_1 z}, \quad z>0 \tag{1}$$

where

$$\beta=\sqrt{k^2-\varepsilon_d\omega^2/c_0^2} \tag{2}$$

is the SPP decay constant normal to the interface into the dielectric, k is the SPP wave vector, ω is the SPP frequency, c_0 is the vacuum speed of light, and ε_d is the permittivity of the dielectric which is given by the complex quantity $\varepsilon_d=\varepsilon_d'+i\varepsilon_d''$. The decay length L of the SPP's into the dielectric is given by

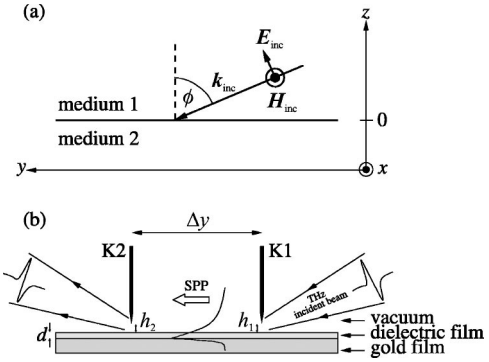

FIG. 1. (a) Schematic of the SPP's incoupling geometry. An electromagnetic wave (wave vector $\boldsymbol{k}_{inc}$) is incident at a angle $\phi=67°$ onto the interface $z=0$ defined by medium 1 (dielectric) and medium 2 (metal). The electric-field vector $\boldsymbol{E}_{inc}$ lies in the plane of incidence, whereas $\boldsymbol{H}_{inc}$ is along x direction). (b) Experimental setup (not to scale) used for exciting SPP's on a gold film of 300 nm thickness covered with a dielectric film of thickness d. The incoming THz beam is focused on the incoupling aperture h_1 which is defined by razor blade $K1$ and the surface of the dielectric. The THz spot diameter at the focus is approximately 1 mm. The SPP's travel along the sample interface until scattered at the outcoupling aperture h_2. The incoupling and outcoupling apertures h_1 and h_2 can be individually varied from 0 to 10 mm by changing the height of $K1$ and $K2$, respectively. The distance Δy between $K1$ and $K2$ defines the SPP's longitudinal propagation distance.

$$L = 1/\mathrm{Re}(\beta). \tag{3}$$

Further, the boundary conditions at $z=0$ yield the SPP dispersion relation[1]

$$k(\omega) = \omega/c_0\sqrt{\varepsilon_m\varepsilon_d/(\varepsilon_m+\varepsilon_d)}, \tag{4}$$

where ε_m denotes the complex permittivity of the metal. The electric field $\boldsymbol{E}(y,z,t)$ of the SPP's can be straightforwardly derived from $\boldsymbol{H}(y,z,t)$. In our experiments the metal is gold and the semi-infinite dielectric is air.

For a dielectric film of thickness d on top of the metal additional boundary conditions apply at $z=d$ and the situation is somewhat more complicated. However, the SPP's still decay exponentially into both air and metal while carrying a certain amount of electromagnetic energy through the film.[13] The decay length L in air increases approximately with the square of the wavelength, i.e., $L \propto \lambda^2$, and with the inverse of the thickness of the dielectric film on top of the metal, i.e., $L \propto d^{-1}$.[13] Therefore, shorter wavelengths are better confined close to the surface than longer wavelengths. For thicker films this confinement becomes even stronger. As shown below, we have proven these dependencies at THz frequencies. Further, the decay length L in air also depends on the dielectric properties of the film,[13] which allows to perform accurate terahertz SPP spectroscopy.

Our experiments are based on a standard THz time-domain spectroscopy setup.[14,15] In such a setup a train of pulses with a duration of 150 fs from Ti:sapphire laser is split into two beams. One of these beams constitutes the excitation beam while the other is the probe beam. The excitation pulses are used to optically generate coherent broadband THz radiation from an InGaAs surface field emitter[16] and the probe pulses gate a photoconductive antenna as receiver.[17] By varying the time delay between the two pulse trains, the THz pulse amplitude can be detected as a function of time with sub-picosecond resolution.

Because the dispersion relations of electromagnetic waves and SPP's do not match for $k \neq 0$ [see Eq. (4)], it is impossible to excite surface plasmons directly by simply illuminating a metal surface. The standard setup was modified to allow the coupling of the free propagating THz radiation into SPP's and to couple out SPP's into THz radiation after they had propagated a variable distance on the sample. An aperture excitation technique[18] was used for the coupling. This technique has the important advantage that it allows broadband coupling. Figure 1(b) illustrates the SPP coupling section of our experimental setup, including SPP incoupling, SPP propagation along the metal surface, and SPP outcoupling. THz radiation incident at an angle of 67° with respect to the sample normal is focused to a small gap defined by the edge of a razor blade (denoted by $K1$) and the sample surface. This blade is at a distance h_1 (denoting the incoupling height) from the sample. This geometry leads to scattering of the incident radiation and the generation of evanescent waves comprising a continuum of wave vectors. As a consequence, the dispersion relations of a fraction of the incident THz radiation and the SPP's match, i.e., coupling becomes possible. The outcoupling is performed by another razor blade $K2$ placed at height h_2 above the sample surface. The outcoupled THz radiation is then guided to the detection antenna.

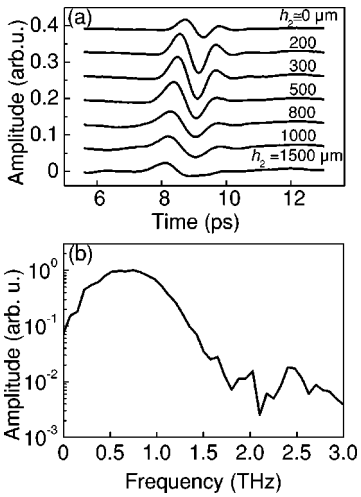

FIG. 2. (a) THz time-domain transients of SPP's having propagated 18 mm along a gold film covered with a 3.8 μm thick dielectric film of cyclotene for different outcoupling heights h_2. The incoupling height (the distance of the incoupler from the sample surface) is kept constant at 300 μm. The transients are offset vertically for clarity. (b) Spectrum obtained by Fourier transforming the time domain signal for $h_2=300$ μm.

For the experiments we use three different samples: a gold surface, a gold surface covered with a dielectric film of cyclotene with a thickness $d=3.8$ μm, and a gold surface with a film of $d=9$ μm of the same dielectric. The films were deposited by spin coating onto the gold surfaces. The gold surfaces were fabricated by evaporating 300 nm of gold onto silicon wafers.

Figure 2(a) presents THz time-domain transients of SPP's propagating 18.0 mm on the gold surface covered with the $d=3.8$ μm thick cyclotene layer. The incoupling height h_1 above the sample surface remains constant at 300 μm for all measurements. The different transients in the figure correspond to different outcoupling heights h_2, varied from $h_2 \simeq 0$ (almost touching the surface) to 1500 μm. For clarity, a vertical offset is introduced in the data of Fig. 2(a). As the outcoupling height is increased the SPP signal increases, reaching a maximum at $h_2 \simeq 300$ μm. This height corresponds to the optimum coupling efficiency. As the height is further increased the signal decreases as result of the decay of the SPP's in air and the decrease of the coupling efficiency.[19] Note that even when $K2$ touches the surface of the sample, i.e., $h_2 \simeq 0$, a signal is observed. This might be attributed to the finite aperture defined by cyclotene layer and to small misalignments of the knife. As can be appreciated in Fig. 2(a) the pulse broadens as h_2 increases. As it is shown below, this broadening is due to a spectral narrowing, resulting from the strong frequency dependence of the SPP decay constant into air.

To further analyze the THz time-domain transients we calculate their Fourier transform. The Fourier spectrum $A(\nu)$ of the largest signal of Fig. 2(a), where $h_1=h_2=300$ μm, is shown in Fig. 2(b). The spectrum extends up to $\simeq 2$ THz,

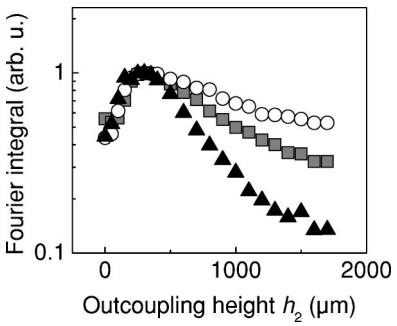

FIG. 3. Fourier integral in the spectral range 0.2–2 THz of the SPP's time-domain transients plotted versus the outcoupling height. The circles correspond to SPP's propagating 18 mm on a bare gold surface. The gray squares belong to SPP's on a gold surface covered with a 3.8 μm thick cyclotene film, and the black triangles to SPP's on a gold surface with a 9 μm thick cyclotene film. All curves are normalized with respect to their maximum values.

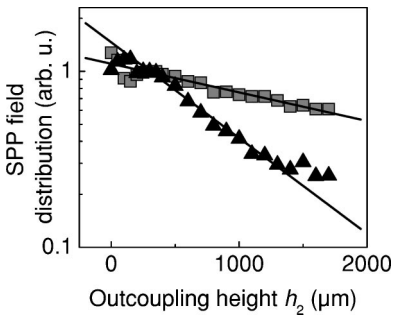

FIG. 4. Surface plasmon polariton field amplitude in air as a function of the height to the sample surface. The gray squares correspond to a gold surface covered with a film of cyclotene of 3.8 μm thickness while the black triangles were measured on a gold surface with a 9 μm thick cyclotene film. The solid lines represent exponential fits to the data.

illustrating the high bandwidth achieved for the excitation and detection of SPP's. The spectra are integrated over a finite frequency interval [0.2, 2 THz] to obtain the Fourier integral $\mathrm{FI}=\int_{\nu_1}^{\nu_2} A(\nu)d\nu$ of the field amplitude in the spectral region were the majority of the THz energy is contained. The FI is a direct measure for the electromagnetic energy which is coupled out and detected.

Figure 3 shows the FI versus the outcoupling height for the bare gold surface (circles), the gold surface with the 3.8 μm thick cyclotene film (gray squares), and the gold surface with the 9 μm thick cyclotene film (black triangles). In all cases $K1$ is kept 300 μm above the sample surface to achieve maximum incoupling efficiency. The data in Fig. 3 are normalized to their respective maximum values. The strong increase of the FI for small h_2 is due to the increase of the coupling efficiency. For all three samples the maxima are reached at $h_2 \simeq 300$ μm. For larger aperture sizes the FI decreases. This decrease is stronger when the thickness of the dielectric film d is larger, indicating that as d becomes larger the SPP is more strongly confined to the interface.

The values of the FI's in Fig. 3 have to be interpreted as the product of the coupling efficiency with the spatial distribution of the SPP's. The coupling efficiency dependence on the aperture size h_2 is not known *a priori*, which hampers the determination of the SPP decay length from the experiments. To overcome this limitation we note that for a bare gold surface and at THz frequencies the SPP air decay length is larger than 16 mm. This decay length can be calculated with Eqs. (2), (4), and (3), and the permittivity of gold at THz frequencies [$\varepsilon'_{\mathrm{m}}=-8.6\times10^4$, $\varepsilon''_{\mathrm{m}}=6.23\times10^5$ at 1 THz (Ref. 20)]; and it is larger by at least a factor of 10 than the decay distance of $\simeq 1.4$ mm obtained from the measurements in the range 300 μm$<h_2<$1500 μm. Hence, the circles in Fig. 3 represent to a good approximation the dependence of the coupling efficiency on h_2. Assuming that this coupling efficiency is the same for the three samples, the differences on the FI's of Fig. 3 are solely due to the spatial distribution of the SPP's. This assumption is justified by the fact that the scattering properties of the surface-knife aperture are not significantly modified by a dielectric film much thinner than the radiation wavelength and aperture size.[19]

Figure 4 depicts the surface plasmon polariton FI's after dividing out the coupling efficiency. The gray squares correspond to the gold surface with the 3.8 μm thick cyclotene film on top and the black triangles to the sample with the 9 μm thick cyclotene film. The experimental values for the SPP decay lengths L_{exp} can be derived by fitting the data of Fig. 4 with the function $\exp(-z/L_{\mathrm{exp}})$. These fits, shown with solid lines in the figure, yield $L_{\mathrm{exp}}=2.7\pm0.6$ mm for the sample with the 3.8 μm thick layer and 0.8 ± 0.1 mm for the one with the 9.0 μm film. It is important to notice that L_{exp} represent broadband values (weighted over the broad spectrum of the THz pulses used). For a comparison with the theoretical values of the decay lengths, the latter have to be calculated for specific frequencies and also weighted over the THz frequency spectrum. This procedure leads to the values $L_{\mathrm{theo}}=2.14$ mm and 0.92 mm, respectively. Within our experimental accuracy we find a very good agreement between the measured and calculated values of the SPP decay length in air. The respective values of L_{exp} and L_{theo} are summarized in Table I.

Information about the frequency dependence of the SPP's decay length can be obtained from the analysis of the spectra. In Fig. 5 we show the SPP's spectra of the 9 μm cyclotene sample for different outcoupling heights h_2, while h_1 is kept constant at 300 μm. For increasing outcoupling heights h_2 we observe a decrease in amplitude in the high-frequency part of the THz spectra. This decrease is due to the frequency dependence of the SPP decay length into air, i.e., high frequencies are confined closer to the sample surface and do not contribute to the signal for large h_2. The spectral narrowing

TABLE I. Dielectric film thickness d, experimental value of SPP's decay length in air, L_{exp}, and the theoretical value of this decay length, L_{w}.

$d(\mu\mathrm{m})$	L_{exp} (mm)	L_{w} (mm)
3.8	2.7 ± 0.6	2.14
9.0	0.8 ± 0.1	0.92

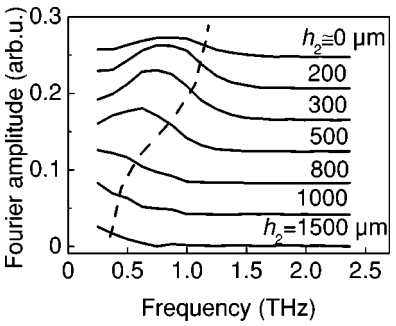

FIG. 5. Fourier spectra (solid lines) for a 300 nm thick gold film covered with 9 μm cyclotene. Every spectrum corresponds to a specific outcoupling height h_2. The incoupler remains at a constant height of 300 μm. The spectra are offset vertically for clarity. The dashed line marks the upper cutoff frequency for each spectrum, i.e., the frequency at which the spectrum has decreased to half of its maximum amplitude.

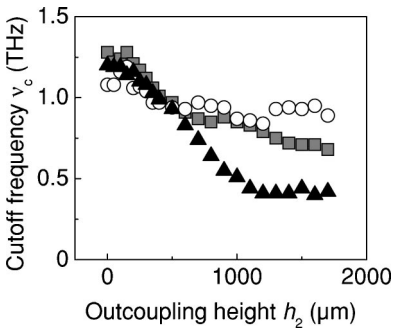

FIG. 6. Surface plasmon polariton cutoff frequency ν_c as a function of the outcoupling height h_2. The open circles correspond to SPP's propagating on a gold surface and the gray squares and the black triangles correspond to gold surfaces covered with cyclotene films of thickness 3.8 μm and 9 μm, respectively.

as a function of h_2 leads to the mentioned pulse broadening of Fig. 2(a). This narrowing can be quantified in terms of the upper cutoff frequency ν_c, i.e., the frequency at which the spectra decrease to half their maximum amplitude. The cutoff frequency is represented in Fig. 5 by the dashed line and in Fig. 6. The data of Fig. 6 correspond to SPP's propagating on the gold surface (open circles), on the gold surface covered with 3.8 μm (gray squares) and 9 μm (black triangles) thick cyclotene film. As can be appreciated in the figure, the cutoff frequency decreases as h_2 increases, and for a fixed h_2 above $\simeq$500 μm the cutoff frequency is lower as the thickness of the cyclotene film increases; in other words high frequencies penetrate less into air than low frequencies and the confinement of the SPP to the surface is better when the thickness of dielectric film is larger.

In conclusion, in this paper we have demonstrated THz time-domain excitation of SPP's. In particular, we have measured the spatial and spectral field distribution of the SPP's above a gold surface. In the presence of a thin dielectric film on top of the metal the SPP field distribution is drastically altered, leading to a strong confinement to the surface. An increase in the dielectric film thickness leads to an even stronger confinement of the SPP's close to the surface. For a constant dielectric film thickness higher frequencies penetrate less into air than lower frequencies. These measurements prove the capabilities of SPP's for THz spectroscopy of thin films. Due to the broadband nature and high sensitivity of this method, it will be of particular interest for the sensing of biomolecules with resonant transitions at THz frequencies on metal surfaces.

The authors gratefully acknowledge helpful discussions with A. Stahl and financial support from the *Deutsche Forschungsgemeinschaft*, the *Ministerium für Schule, Wissenschaft und Forschung des Landes Nordrhein-Westfalen*, and by the European Union through the TMR project *Interaction*.

*Electronic address: rivas@iht.rwth-aachen.de

[1] H. Raether, *Surface Plasmons on Smooth and Rough Surfaces and on Gratings* (Springer-Verlag, Berlin, 1988).
[2] T.W. Ebbesen, H.J. Lezec, H.F. Ghaemi, T. Thio, and P.A. Wolff, Nature (London) **391**, 667 (1998).
[3] L. Martín-Moreno, F.J. García-Vidal, H.J. Lezec, K.M. Pellerin, T. Thio, J.B. Pendry, and T.W. Ebbesen, Phys. Rev. Lett. **86**, 1114 (2001).
[4] W.L. Barnes, A. Dereux, and T.W. Ebbesen, Nature (London) **424**, 824 (2003).
[5] P. Haring Bolívar, in *Semiconductor Quantum Optoelectronics*, edited by A. Miller, M. Ebrahimzadeh, and D.M. Finlayson (Institute of Physics Publishing, London, 1999), pp. 151–192.
[6] B. Ferguson and X.-C. Zhang, Nat. Mater. **1**, 26 (2002).
[7] M. Brucherseifer, M. Nagel, P. Haring Bolívar, H. Kurz, A. Bosserhoff, and R. Büttner, Appl. Phys. Lett. **77**, 4049 (2000).
[8] M. Bykhovskaia, B. Gelmont, T. Globus, D.L. Woolard, A.C. Samuels, T.H. Duong, and K. Zakrzewska, Theor. Chem. Acc. **106**, 22 (2001).
[9] M. Nagel, P. Haring Bolívar, M. Brucherseifer, H. Kurz, A. Bosserhoff, and R. Büttner, Appl. Phys. Lett. **80**, 154 (2001).
[10] B.M. Fischer, M. Walther, and P. Uhd Jepsen, Phys. Med. Biol. **47**, 3807 (2002).
[11] J. Gómez Rivas, C. Schotsch, P. Haring Bolívar, and H. Kurz, Phys. Rev. B **68**, 201306(R) (2003).
[12] J. P. Vigneron, in *Near Field Optics*, edited by D. W. Pohl and D. Courjon (Kluwer Academic, Dordrecht, 1993), pp. 147–156.
[13] I.P. Kaminow, W.L. Mammel, and H.P. Weber, Appl. Opt. **13**, 396 (1974).
[14] D.R. Grischkowsky, S. Keiding, M. van Exter, and C. Fattinger, J. Opt. Soc. Am. B **7**, 2006 (1990).
[15] M. van Exter and D.R. Grischkowsky, IEEE Trans. Microwave Theory Tech. **38**, 1684 (1990).
[16] X.-C. Zhang and D.H. Auston, J. Appl. Phys. **71**, 326 (1992).
[17] D.H. Auston, K.P. Cheung, and P.R. Smith, Appl. Phys. Lett. **45**, 284 (1984).
[18] E.V. Alieva, G. Beitel, L.A. Kuzik, A.A. Sigarev, V.A. Yakovlev, G.N. Zhizhin, A.F.G. van der Meer, and M.J. van der Wiel, Appl. Spectrosc. **51**, 584 (1997).
[19] G.N. Zhizhin, S.F. Parker, M.A. Chesters, and V.A. Yakovlev, Opt. Spectrosc. **65**, 223 (1988).
[20] M.A. Ordal *et al.*, Appl. Opt. **22**, 1099 (1983).